IEEE Access
Multidisciplinary | Rapid Review | Open Access Journal

Received June 1, 2020, accepted June 23, 2020, date of publication June 30, 2020, date of current version July 20, 2020.

Digital Object Identifier 10.1109/ACCESS.2020.3006022

Time-Varying RFI Suppression of Dechirping Radar Based on l_1 Norm Filtering and RAM-Based Frequency Estimation

PENGCHENG WAN, NINGNING TONG, AND GUIMEI ZHENG, (Member, IEEE)
Air and Missile Defense College, Air Force Engineering University, Xi'an 710051, China

Corresponding author: Pengcheng Wan (wppcheng@163.com)

This work was supported in part by NSFC under Grant 61571459, Grant 61631019, and Grant 61701526.

ABSTRACT This paper presents a novel framework for suppressing time-varying radio frequency interference (TRFI) in wideband dechirping radar. The TRFI challenges the wideband radar because of 1) changing in wide spectra range; 2) dynamic nature and unpredictability; 3) significant noise power in limited band. In this paper, an essential phenomenon of real measured data about TRFI in dechirping process is analyzed, where it is smashed into several segments because of the narrowband filtering. Based on that, a 2-step framework combining the interference filtering and frequency estimation is proposed. First, since the different sparsity of signal of interference, a simple yet very effective regional filtering method based on l_1 norm of STFT is applied, which transforms original problem into a sparse signal recovery problem. Second, for 1-D signal, the reweighted atomic norm minimization (RAM) algorithm is applied to estimate the signal from defect filtered data; for 2-D signal block, a weighting strategy is proposed to promote the accuracy of original 2-D atomic norm minimization method. This method can be implemented as an interference suppression stage for wideband radar with dechirping processing. Experiment of real measured signal in TRFI environment and simulation of defect signal block illustrate its effectiveness.

INDEX TERMS Sparse recovery, reweighted atomic norm minimization (RAM), radio frequency interference (RFI), dechirping.

I. INTRODUCTION

The bandwidth of high-resolution radar usually ranges from 100 MHz to several GHz, which is easily influenced by time-varying radio frequency interference (TRFI) [1], characterized by instantaneous frequency laws changing in time domain. These interferences can be either narrowband or wideband [2]–[10], and their center frequencies hardly follow a pattern. The RFI [11]–[16] is usually caused by signals of television, mobile communications, radio, and cellular phones, *et al*. With the electromagnetic spectrum becoming increasingly congested, there are also some intentional interference such as frequency-sweeping jammer, which quickly changes in time domain and is extremely hard to suppress. In this paper, these interferences are all classified as TRFI.

Because of the dynamic nature and unpredictability, the TRFI is very challenging to suppress. Previous work in RFI suppression area can be classified into two following categories.

1) Suppression via filtering techniques, where the received signal is processed by a notch filter or adaptive filter to mitigate the interference source to noise floor, which is popular in practical implementations because it is easy to realize.

2) Interference extraction, including methods of eigen decompositions [7], [8], spectral decomposition [15], independent component analysis [6], time-frequency analysis [5], [17], where the RFI components are first detected and estimated, and then subtracted from the received signal. In [2], a modified component analysis method using complex tensor is proposed, which is designed to mitigate continuously distributed NBIs and WBIs simultaneously. A signal reconstruction method based on dynamic synthetic aperture scheme is proposed for suppressing deceptive jamming in [18].

Recently, the sparse recovery method has been utilized in interference mitigation area [13], but requires prior knowledge to build a representation dictionary, which cannot

The associate editor coordinating the review of this manuscript and approving it for publication was Prakasam Periasamy.

adapt dynamic TRFI. This problem is further solved in [14] by adding an initial estimation step that operates directly on a contaminated radar signal to identify the interference primary subband.

However, there are still problems exist. First, the suppression by filtering will have a negative effect on the signal power, and the sidelobe will be introduced, leading to serious associated problems [14]. Second, the main difficulty of the latter TRFI-extraction method is that the data collected has been heavily contaminated by strong noise. Therefore, unless there is very accurate prior information about the TRFI source, it is hard to model or estimate the interference effectively. The dynamic range and sampling resolution of equipment also limit realization of such methods, even though they are theoretically feasible.

A crucial phenomenon ignored by most interference extraction methods is that dechirping has thoroughly changed the frequency and bandwidth of original TRFI. Dechirping for large bandwidth linear frequency modulation (LFM) signal is a universal technic in high resolution radar system [19], [20], after which the dynamic frequency interference will not remain intact with complete frequency but become isolated as several blocks in time domain. More details will be covered in section II, where we will analyze this phenomenon in detail.

A defect for filtering technic is that the signal becomes incomplete and sparse, which is the reason for low power and sidelobe. Recently, the emerging super-resolution method stimulate numerous investigations on sparse signal recovery. Reference [21] first proposed a compressive sensing method for radar imaging. Then the sparse recovery method was used for super-resolution [22]–[27], including sparse Bayesian learning [24], 2D gradient projection [25], matrix completion [26], atomic norm minimization (ANM) [28], [29], reweighted atomic norm minimization (RAM) [27], [30], *et al*. Among those methods, the RAM has shown great advantage in estimation accuracy [27], [30], [31] because of the off-grid characteristic and high estimation accuracy.

In this paper, we investigate the change of TRFI from basic of dechirping, and a notching method based on l_1 norm after short-time Fourier transform (STFT) is proposed to transform it into a typical sparse recovery problem. After that, the RAM is applied for 1-D and 2-D frequency estimation. Our main novel contributions are listed as follows.

1) The interference phenomenon of TRFI on dechirping is explained by investigating the interference mechanism from the basic, and find that the interference has been changed and smashed by dechirping and filtering, which is different from the suppose of some interference extraction methods such as [2].

2) The proposed TRFI filtering method based on l_1 norm analysis after STFT is efficient and performs well in strong TRFI.

3) The RAM-based line spectrum estimation for filtered signal is verified by a real experiment with TRFI.

4) We further promote the ANM for 2D data by implementing a weighting strategy, which effectively improved the calculation accuracy.

Organization wise, Section II provides details on signal and TRFI modeling, as well as basic dechirping. Section III presents our main proposed approach for filtering and RAM-based frequency estimation. Section IV presents experiments to verify the effectiveness of proposed method.

II. DECHIRPING OF SIGNAL AND INTERFERENCE

Dechirping is a pulse compression technique for LFM, which is widely applied in radar imaging system such as SAR and ISAR. It transforms the signal bandwidth into a few hundred of the original in analog electronic devices, extraordinarily reducing the requirement for the analog-to-digital converter (ADC). Flowchart of dechirping is shown in Figure 1.

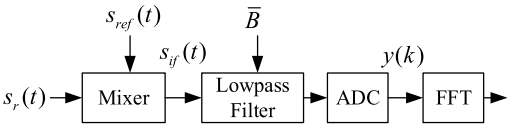

FIGURE 1. Block diagram of dechirping for LFM.

In order to better illustrate the interference mechanism of TRFI, we start from the basic of dechirping. Suppose the radar transmits a LFM signal, then the echo of target $s_r(t)$ with a distance of R_t will be

$$s_r(t) = A\text{rect}\left(\frac{t - 2R_t/c}{T_p}\right) e^{j2\pi\left(f_c\left(t-\frac{2R_t}{c}\right)+\frac{1}{2}\gamma\left(t-\frac{2R_t}{c}\right)^2\right)} \tag{1}$$

where $\text{rect}(u) = \begin{cases} 1 & |u| \le \frac{1}{2} \\ 0 & |u| > \frac{1}{2} \end{cases}$, f_c is the center frequency, T_p is the pulse width, $\gamma = B/T_p$ and t is the time.

Dechirping is a method using a LFM signal with the center frequency of f_c and the chirp rate of $-\gamma$ as the reference to mix the echo for frequency difference processing. The reference is

$$s_{ref}(t) = \text{rect}\left(\frac{t - 2R_{ref}/c}{T_{ref}}\right) e^{j2\pi\left(f_c\left(t-\frac{2R_{ref}}{c}\right)+\frac{1}{2}\gamma\left(t-\frac{2R_{ref}}{c}\right)^2\right)} \tag{2}$$

where R_{ref} is the reference range, which indicates the center of the observed area, and T_{ref} is the pulse width of reference, usually wider than T_p. The output of mixer is $s_{if}(t) = s_r(t) \cdot s^*_{ref}(t)$

$$s_{if}(t) = A\text{rect}\left(\frac{t - 2R_t/c}{T_p}\right) e^{-j\frac{4\pi}{c}\gamma(t-\frac{2R_{ref}}{c})R_\Delta - j\frac{4\pi}{c}f_cR_\Delta + j\frac{4\pi\gamma}{c^2}R_\Delta^2} \tag{3}$$

where $R_\Delta = R_t - R_{ref}$ and the $s_{if}(t)$ is a single frequency pulse whose frequency is proportional to R_Δ. If the required observation range is $[R_{ref} - \Delta r/2, R_{ref} + \Delta r/2]$, the frequency range will be $[-\gamma\Delta r/c, \gamma\Delta r/c]$, which means the bandwidth of signal will be transformed into $\overline{B} = 2\gamma\Delta r/c = B\Delta r/R_p$, where R_p is the corresponding range of T_p. Then, the s_{if} will be input into a lowpass filter with bandwidth equal or slightly greater than $\overline{B}$, then the output will be collected by ADC for fast Fourier transform (FFT) to show the spectrum, where the frequencies corresponds to spatial ranges. Figure 2 indicates the signal and TRFI before and after dechirping in time-frequency domain.

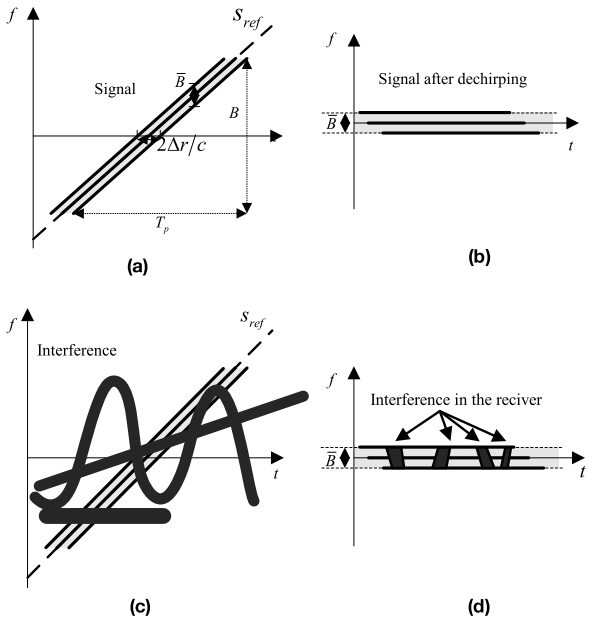

FIGURE 2. Signal and TRFI before and after dechirping in time-frequency domain. (a) Typical original LFM signals. (b) Signals after dechirping. (c) Signal together with TRFI. (d) Signals and TRFI after dechirping.

The TRFI is modeled as

$$i(t) = A_i(t)e^{j(2\pi f_{ci}(t)t+\varphi_i(t))} \tag{4}$$

where $f_{ci}(t)$ is the interference frequency which follows an arbitrary pattern, $A_i(t)$ denotes the noise amplitude and $\varphi_i(t)$ is the phase. For concentration of interfering energy, the bandwidth of TRFI is usually limited. The output of mixer is

$$\begin{aligned} i_{if}(t) &= i(t)\cdot s^*_{ref}(t) \\ &= A_i \mathrm{rect}\left(\frac{t-2R_{ref}/c}{T_{ref}}\right) \\ &\quad \cdot e^{j2\pi\left((f_{ci}-f_c)t+\varphi_i+\frac{2f_cR_{ref}}{c}-\frac{\gamma}{2}\left(t-\frac{2R_{ref}}{c}\right)^2\right)} \end{aligned} \tag{5}$$

The whole interference cannot be acquired totally because of the lowpass filter. After the filter, a narrow band noise will be collected, whose bandwidth is usually not the whole bandwidth of original interference and is equal to or narrower than the filter bandwidth. This is the main reason for the defect of interference extraction methods, which can hardly be realized in LFM dechirping systems because of the incompletion of TRFI after dechirping.

The collected digital signal from ADC is

$$y(k) = x(k) + i(k) + n(k), \quad k = 1, 2, \ldots K \tag{6}$$

where k denotes the index of range sample, $x(k)$ denotes the collected signal, $i(k)$ denotes the interference and $n(k)$ denotes an additive noise. Figure 3 simulates each step of dechirping, where the first column is LFM and the second is NRI.

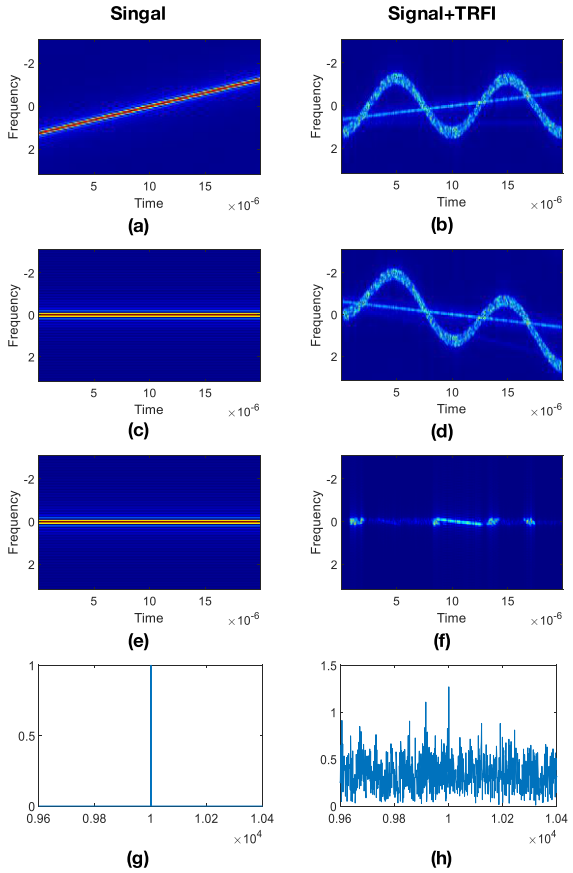

FIGURE 3. Each step of dechirping, where the first column is LFM and the second is NRI. (a) and (b) are the STFT of original LFM and NRI; (c) and (d) are the STFT of mixer output, where the slopes have been changed; (e) and (f) are the STFT of filter output, where the original NRI has been changed into a narrowband interference; (g) and (h) are the outputs in frequency domain, where (h) has been severely interfered that signal has been buried in noise.

III. PROPOSED METHOD

Proposed method combines interference filtering approach and spectrum estimation method. As verified in [30], [31], the RAM shows great performance in sparse signal recovery. Proposed method includes following steps. 1) Interference filtering based on l_1 norm of STFT, which transforms the problem into a common sparse signal recovery problem. 2) 1-D or 2-D spectrum estimation of filtered data based on RAM.

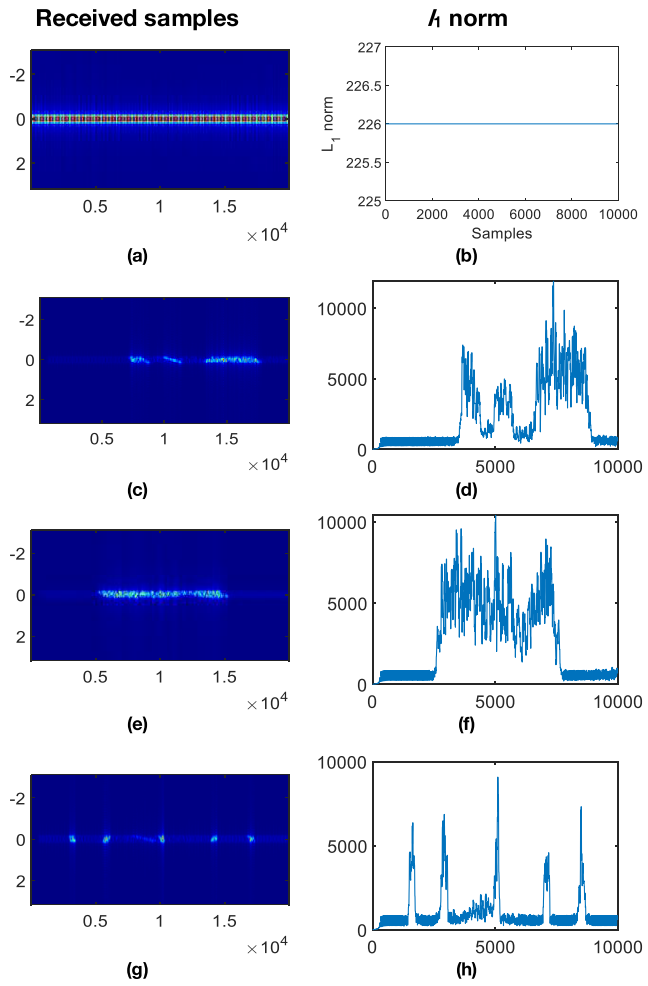

FIGURE 4. STFT of received samples (first column) and their corresponding l_1 norm (second column).

A. INTERFERENCE FILTERING BASED ON l1 NORM OF STFT

A common phenomenon is that, the noise interference after sampling shows discrete block distribution in time domain, and frequency energy distribution of the noise block is denser than signal owing to containing more frequency components. According to the property, the time-frequency distribution of the received signal is analyzed, and a simple but effective filtering method is proposed. The STFT with rectangular window of length M can be formulated as

$$\boldsymbol{STFT} = [STFT(k,l)] = \left[\sum_{m=0}^{M-1} y(k+m)e^{-j2\pi lm/M}\right] \quad (7)$$

which can be written in vector form as

$$\boldsymbol{STFT} = [\boldsymbol{\rho}(1), \boldsymbol{\rho}(2)\cdots\boldsymbol{\rho}(k)\cdots] \quad (8)$$

where $\boldsymbol{\rho}(k)$ denotes the transformed vector of k th index.

The l_1 norm is sensitive to the sparsity of vectors and is widely used in sparse reconstruction algorithms. Here we apply it to the detection of interference region. According to previous analysis, the interference after dechirping is relatively dense in frequency domain, whereas the signal is relatively sparse.

The l_1 norm of $\boldsymbol{\rho}(k)$ is calculated by

$$\begin{aligned}\boldsymbol{L}(k) = L_1\boldsymbol{\rho}(k) &= \left\|\sum_{m=0}^{M-1} y(k+m)e^{-j2\pi lm/M}\right\|_1 \\ &= \sum\nolimits_l \left|\sum_{m=0}^{M-1} y(k+m)e^{-j2\pi lm/M}\right| \end{aligned} \quad (9)$$

The interference region is much more intense in frequency domain than signal region, corresponding to the l_1 norm, where $\boldsymbol{L}_{1\text{interference}} \gg \boldsymbol{L}_{1\text{signal}}$. This criterion determines whether $y(k)$ is an interference or a signal. A binary hypothesis can be established, where $H_0 : y(k)$ is signal and $H_1 : y(k)$ is interference. σ is a threshold and $\sigma = \lambda L_s$, where L_s is the pure signal l_1 norm, which is estimated by the first several l_1 norm results where the pure signal region shows a stable characteristic. λ is a constant between 2 to 4 according to the interference power. The value setting of σ rely on first several results to analyze and conduct an estimation of interference and signal regions. After that, we can utilize it automatically.

$$\begin{cases}\boldsymbol{L}(k) \le \sigma, & H_0 \text{ is true} \\ \boldsymbol{L}(k) > \sigma, & H_1 \text{ is true}\end{cases} \quad (10)$$

Because of noise has the characteristics of instability, there are large fluctuations in individual positions of direct calculated $\boldsymbol{L}(k)$, bringing intolerable errors. To solve this problem, a sliding window detection method is constructed as

$$\begin{aligned}\boldsymbol{L}_W(k) &= \|[\boldsymbol{\rho}(k), \cdots \boldsymbol{\rho}(k+1)\cdots, \boldsymbol{\rho}(k+K)]\|_1 \\ &= \max_{k_i\in[k,k+K]} L_1\boldsymbol{\rho}(k_i)\end{aligned} \quad (11)$$

and (10) is transformed to

$$\begin{cases}\boldsymbol{L}_W(k) \le \sigma, & H_0 \text{ is true} \\ \boldsymbol{L}_W(k) > \sigma, & H_1 \text{ is true}\end{cases} \quad (12)$$

This smoothing method can effectively avoid the instability of individual positions. After detection, the filtering criterion will be (13), which transforms original data to a typical sparse data.

$$\bar{y}(k) = \begin{cases} y(k), & k \to H_0 \\ 0, & k \to H_1 \end{cases} \quad (13)$$

B. 1-D SPECTRUM ESTIMATION BASED ON RAM

Through previous processing, the interference suppression has been transformed into a typical sparse signal reconstruction problem. Then the RAM-based algorithm is applied to deal with such problems.

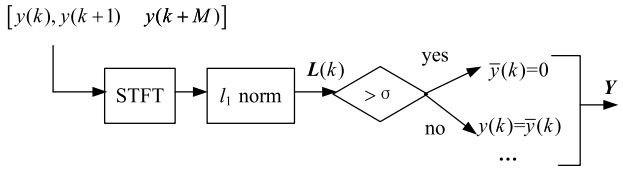

FIGURE 5. Block diagram of TRFI l_1 norm filtering.

The ideal signal is a stack of frequencies with different amplitudes, which can be expressed as

$$\|\boldsymbol{Y}\|_{\mathcal{A},0} = \inf_{f_q,\sigma_q} \left\{ U : \boldsymbol{Y} = \sum_{q=1}^{U-1} \boldsymbol{a}\left(f_q\right)\sigma_q \right\} \tag{14}$$

where σ_q denotes the amplitude of qth frequency index and $\boldsymbol{a}(f) = \left[1, e^{j2\pi f}, \ldots, e^{j2\pi(K-1)f}\right]$ denotes a discrete sinusoid with frequency f. It can be transferred into the following optimization problem

$$\min_{\boldsymbol{u}} \ln|T(\boldsymbol{u}) + \varepsilon \boldsymbol{I}| + tr\left(\boldsymbol{Y}^H T(\boldsymbol{u})^{-1}\boldsymbol{Y}\right) \quad s.t. T(\boldsymbol{u}) \geq 0 \tag{15}$$

where $\boldsymbol{u}$ is a $K \times 1$ vector and $T(\boldsymbol{u})$ is the Toeplitz matrix of $\boldsymbol{u}$. The $rank(\cdot)$ and $tr(\cdot)$ denotes the rank and trace of a matrix. $\varepsilon \boldsymbol{I}$ is a disturbance component to avoid $T(\boldsymbol{u})$ being a singular matrix.

In [32], the RAM is proposed to improve the accuracy by an iterative weighting algorithm. A weighted continuous dictionary is defined as

$$\mathcal{A}^w \triangleq \left\{ \boldsymbol{a}^w(f) = w(f)\boldsymbol{a}(f) \right\} \tag{16}$$

where $w(f)$ is a weighting function. For ith iteration, $w_i(f) = \left(\boldsymbol{a}(f)^H \boldsymbol{W}_i \boldsymbol{a}(f)\right)^{-\frac{1}{2}}$ and $\boldsymbol{W}_i = \left(1/K\right)\left(T(\boldsymbol{u}_i) + \varepsilon \boldsymbol{I}\right)^{-1}$. The weighting function $\boldsymbol{W}_i$ is updated based on the latest solution $\boldsymbol{u}_i$. The final optimization problem for RAM is

$$\begin{aligned} \|\boldsymbol{Y}\|_{\mathcal{A}^w} = \min_{\boldsymbol{u}} \frac{\sqrt{K}}{2}\mathrm{tr}\left(\boldsymbol{W}T(\boldsymbol{u})\right) + \frac{1}{2\sqrt{K}}\mathrm{tr}\left(\boldsymbol{Y}^H T(\boldsymbol{u})^{-1}\boldsymbol{Y}\right) \\ \text{s.t.} T(\boldsymbol{u}) \geq 0 \end{aligned} \tag{17}$$

It can be restored with a standard semidefinite programming (SDP) solver SDPT3 in CVX toolbox. The proof of the above theorem can refer to [32].

C. PROMOTED 2-D SPECTRUM ESTIMATION

The 2-D frequency estimation is extremely useful in radar signal processing such as SAR/ISAR imaging after dechirping and 2-D direction of arrival (DOA) estimation. The 2-D data is usually composed by n_2 1-D signal vectors, formulated as $\boldsymbol{Y} = \left[\boldsymbol{y}_1, \boldsymbol{y}_2 \cdots \boldsymbol{y}_i \cdots \boldsymbol{y}_{n_2}\right] \in \mathbb{C}^{n_1 \times n_2}$, where $\boldsymbol{y}_i$ is a filtered sparse vector with dimension of n_1.

The approximate solution of [34] is based on atomic l_0 norm, which can find the best optimal solution. However, its solution procedure is usually nonconvex. Reference [35] provides an alternative solution to transform atomic l_0 norm into a convex problem. In actual situation, the frequency components are usually not uniformly distributed, and we can approach the most accurate value by an iterative algorithm, which is the same in 2-D case. Based on [32], [35], we extend traditional RAM for line spectrum estimation to the 2-D application.

According to [34], the 2-D matrix $\boldsymbol{Y}$ can be vectorized as $\boldsymbol{z} = \mathrm{vec}\left(\boldsymbol{Y}^{\mathrm{T}}\right) \in \mathbb{C}^{n_1 n_2}$ to transform original problem into a 1-D form. First, we define a continuous dictionary on 2 frequency dimensions as

$$\mathcal{A}^w \triangleq \left\{ \boldsymbol{a}^w(f_1, f_2) = w(f_1, f_2)\boldsymbol{a}(f_1) \otimes \boldsymbol{a}(f_2) \right\} \tag{18}$$

where $\otimes$ denotes the Kronecker product and we have $\boldsymbol{a}(f_1, f_2) = \boldsymbol{a}(f_1) \otimes \boldsymbol{a}(f_2)$;$w(f_1, f_2)$ is a weighting function of f_1 and f_2.

In order to conduct the 2-D reweighted atomic norm minimization frequency estimation, we must solve the following problem

$$\begin{aligned} &\|\boldsymbol{z}\|_{\mathcal{A}^w} \\ &= \inf_{f_{1q}, f_{2q}, \sigma_q^w} \left\{ \sum_q \left\|\sigma_q^w\right\|_2 : \boldsymbol{z} = \sum_q \sigma_q^w \boldsymbol{a}^w\left(f_{1q}, f_{2q}\right) \right\} \\ &= \inf_{f_{1q}, f_{2q}, \sigma_q} \left\{ \sum_q \frac{\|\sigma_q w\|_2}{w(f_1, f_2)} : \boldsymbol{z} = \sum_q \sigma_q \boldsymbol{a}\left(f_{1q}\right) \otimes \boldsymbol{a}\left(f_{2q}\right) \right\} \end{aligned} \tag{19}$$

The weighting function for ith iteration is

$$w_i(f_1, f_2) = \left(\left(\boldsymbol{a}(f_1, f_2)\right)^H \boldsymbol{W}_i \boldsymbol{a}(f_1, f_2) \right)^{-\frac{1}{2}} \tag{20}$$

where $\boldsymbol{W}_i = \left(1/n_1 n_2\right)\left(T(\boldsymbol{U}) + \varepsilon \boldsymbol{I}\right)^{-1} \in \mathbb{C}^{n_1 n_2}$ and $T(\boldsymbol{U})$ is a double-fold Toeplitz structure from a $n_1 n_2$ matrix $\boldsymbol{U} = \left\{u_{m_1, m_2}\right\}(m_1 < n_1, m_2 < n_2)$ [34], composed by

$$T(\boldsymbol{U}) = \begin{bmatrix} \boldsymbol{U}_0 & \boldsymbol{U}_1 & \cdots & \boldsymbol{U}_{n_1-1} \\ \boldsymbol{U}_1^H & \boldsymbol{U}_0 & \cdots & \boldsymbol{U}_{n_1-2}^H \\ \vdots & \vdots & \ddots & \vdots \\ \boldsymbol{U}_{n_1-1}^H & \boldsymbol{U}_{n_1-2}^H & \cdots & \boldsymbol{U}_0 \end{bmatrix} \in \mathbb{C}^{n_1 n_2 \times n_1 n_2} \tag{21}$$

The lth row of $\boldsymbol{U}$ defines $\boldsymbol{U}_l$

$$\boldsymbol{U}_l = \begin{bmatrix} u_{l,0} & u_{l,-1} & \cdots & u_{l,n_2-1} \\ u_{l,1}^H & u_{l,0} & \cdots & u_{l,n_2-2} \\ \vdots & \vdots & \ddots & \vdots \\ u_{l,n_2-1}^H & u_{l,(n_2-2)}^H & \cdots & u_{l,0} \end{bmatrix} \tag{22}$$

Referring (17), the extended solution for (19) is

$$\begin{aligned} &\min_{\boldsymbol{U}} \frac{\sqrt{n_1 n_2}}{2}\mathrm{tr}\left(\boldsymbol{W}T(\boldsymbol{U})\right) + \frac{1}{2\sqrt{n_1 n_2}}\mathrm{tr}\left(\boldsymbol{z}^H T(\boldsymbol{U})^{-1}\boldsymbol{z}\right) \\ &\text{s.t. } T(\boldsymbol{U}) \geq \boldsymbol{0} \end{aligned} \tag{23}$$

The proof of (23) is given in Appendix. By (23), we further apply the reweighting method to guarantee a better precision. Procedure for solving (23) is an iterative algorithm, where the current iteration is based on result of former iteration. Because the problem has been transformed to 1-D, proposed weighting function method is an extension of RAM. We can

also use an SDP solver to deal with optimal problem of (23). Compared with non-weighted method, the reweight method will obtain higher estimation accuracy at the cost of calculating time over several iterations.

However, the complexity will increase rapidly with 2-D ANM-based methods because solving of which is through an SDP solver, which consumes most time, compared to which the computing time of other steps can be ignored. According to [36], the computational complexity of SDP is $O(N^{4.5})$, which means as the number of calculating points increases, the computational complexity grows exponentially. Then, the reality of all 2-D ANM-based methods has to face the limit of computing power. Although complexity has increased, it is tolerable in some small sample cases considering its precision for frequency estimation.

IV. NUMERICAL EXPERIMENTS

In this section, the experiment and simulation results are presented to demonstrate the effectiveness of the proposed method with TRFI environment. Firstly, an experiment for line spectrum estimation in produced TRFI environment is conducted, by applying RAM, we can easily recover the original frequencies. Secondly, we generate a 2-D interfered signal block with random 2-D frequency, and conduct a simulation based on proposed 2-D RAM method.

As to dechirping radars, frequency estimation is the dual problem of signal recovery by implementing inverse FFT. The output root-mean-square error (RMSE) is formulated for evaluating algorithm performance as

$$RMSE = \|\boldsymbol{X} - \boldsymbol{Y}\|_F \big/ \|\boldsymbol{X}\|_F \tag{24}$$

where $\boldsymbol{X}$ is the original signal, $\boldsymbol{Y}$ is the recovered signal after interference region removing and $\|\cdot\|_F$ denotes the Frobenius norm.

A. EXPERIMENT OF 1-D MEASURED DATA

An experiment is conducted to validate the proposed method. The experiment setup is shown in Fig. 6 (a), where a generator working on ARB mode transmits simulated targets signal, which is consisted by sum of 10 LFM signals with random micro delays and powers. The Local Oscillator provides a reference frequency for receiver, which is trigged by the pulse of transmitter for synchronization. The center frequency of LFM signal is 10 GHz and the bandwidth is 100 MHz. Sampling frequency of receiver is 10 MHz. The NRI is a noise with bandwidth of 10 MHz, whose center frequency randomly changes from 0.9 to 10.1 GHz, transmitted by a X-band jammer. Dechirping for received signal is conducted in the receiver with reference frequency. Received segment contains 80 complex indexes.

The STFT of original signal is shown in Figure 7 (a), where the interference region presents more intensive and complex. About 40% of original signal is polluted by 2 jamming segments, where the interference regions have a SINR of -27.3 dB. Through l_1 norm filtering, the severely interfered part can be easily removed. We use integrity rate to describe

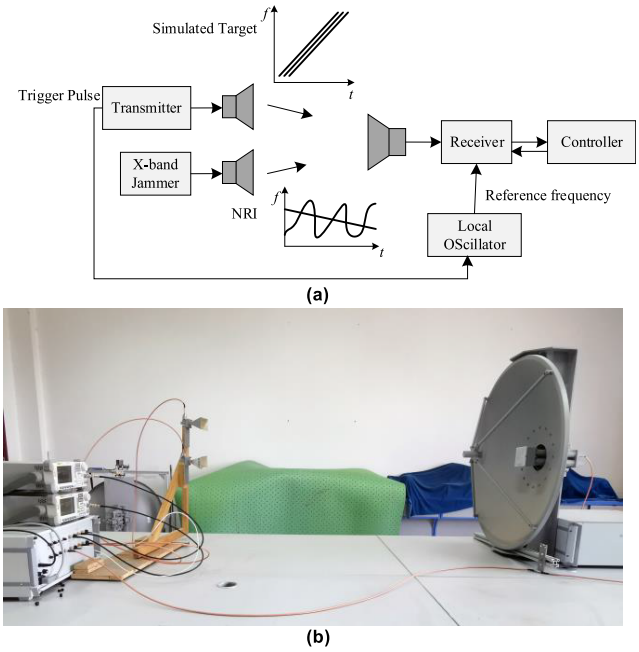

FIGURE 6. (a) Setup for experiment. (b) The scene of experiment.

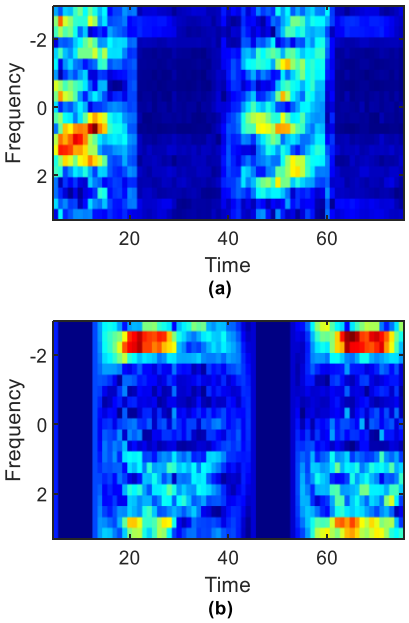

FIGURE 7. (a) STFT of original signal (including interference). (b) STFT of signal after filtering.

the integrity of signal left after interference removing and here the integrity rate is 58%. Figure 7 (b) shows the STFT of filtered signal, where only some signal segments left.

Dechirping for received signal is conducted in the receiver with reference frequency. Received segment contains 80 complex indexes. The STFT of original signal is shown in Figure 7 (a), where the interference region presents more intensive and complex. About 40% of original signal is polluted by 2 jamming segments, where the interference

regions have a SINR of −27.3 dB. Through l_1 norm filtering, the severely interfered part can be easily removed. We use integrity rate to describe the integrity of signal left after interference removing and here the integrity rate is 58%. Figure 7 (b) shows the STFT of filtered signal, where only some signal segments left.

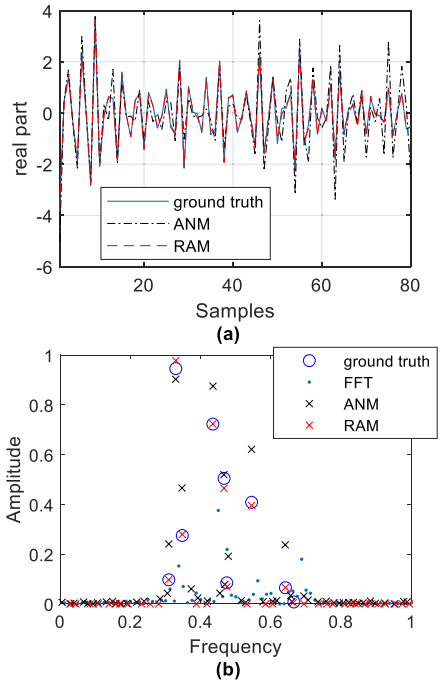

FIGURE 8. Recovery results. (a) Real part of recovered signal. (b) Recovered spectra of FFT, ANM and RAM.

Next, the essential step is to recover the complete signal and estimate the frequencies from defective data. The ANM and RAM are tested for super resolution frequency estimation, where the conventional FFT is also used for comparison. Figure 8 shows the recovery results, and the RAM shows best accuracy in proposed situation, after 3 iterations. In Figure 8 (b), the FFT loses its efficacy in such situation where the estimation result can hardly match the ground truth and sidelobes has been introduced to cause the degradation of resolution, which is the real situation for some directly filtering algorithms. The estimated spectra of RAM match the ground truth well, whereas the ANM shows greater error. The results preliminarily verify the effectiveness of RAM and ANM for recovering the defect data.

A significant factor of the results is integrity rate which is the base of data recovery. Thus, 50 Carlo experiments about the RMSE of ANM and RAM against different integrity rate (from 10% to 100%) are conducted and the result is shown in Figure 9 (a). In the case, RAM and ANM will successfully work when integrity rate is higher than 30% and RAM shows better performance considering its RMSE is much lower than ANM. Notice that the needed integrity rate depends on the number of signals, which has shown in [32]. Furthermore, an experiment to illustrate the RMSE against SINR under

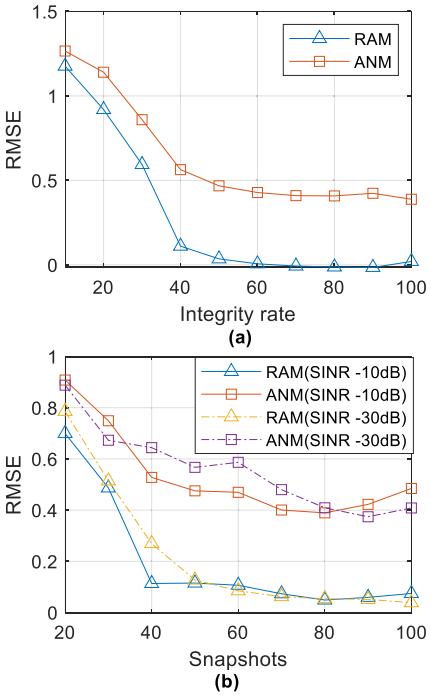

FIGURE 9. RMSE of RAM and ANM. (a) RMSE under different integrity rate. (b) RMSE against SINR under different snapshots.

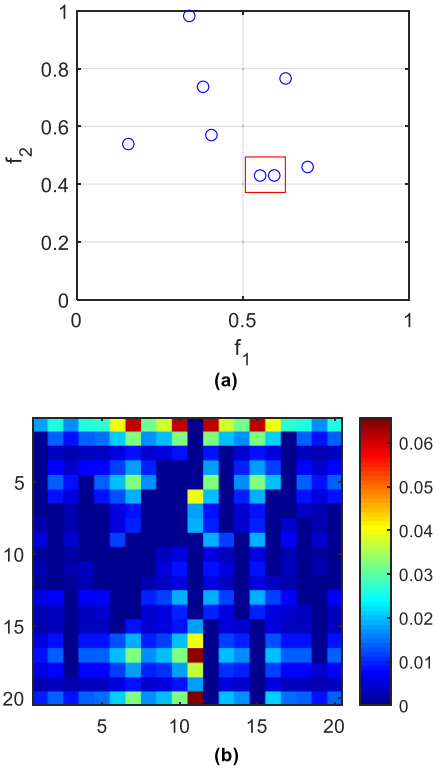

FIGURE 10. (a) Real locations of (f_1, f_2). (b) Amplitude of simulated filtered signal block, where each column presents banded sparsity in random position.

different snapshots is conducted. The SINR here is defined as the signal-interference-plus-noise ratio in interference region,

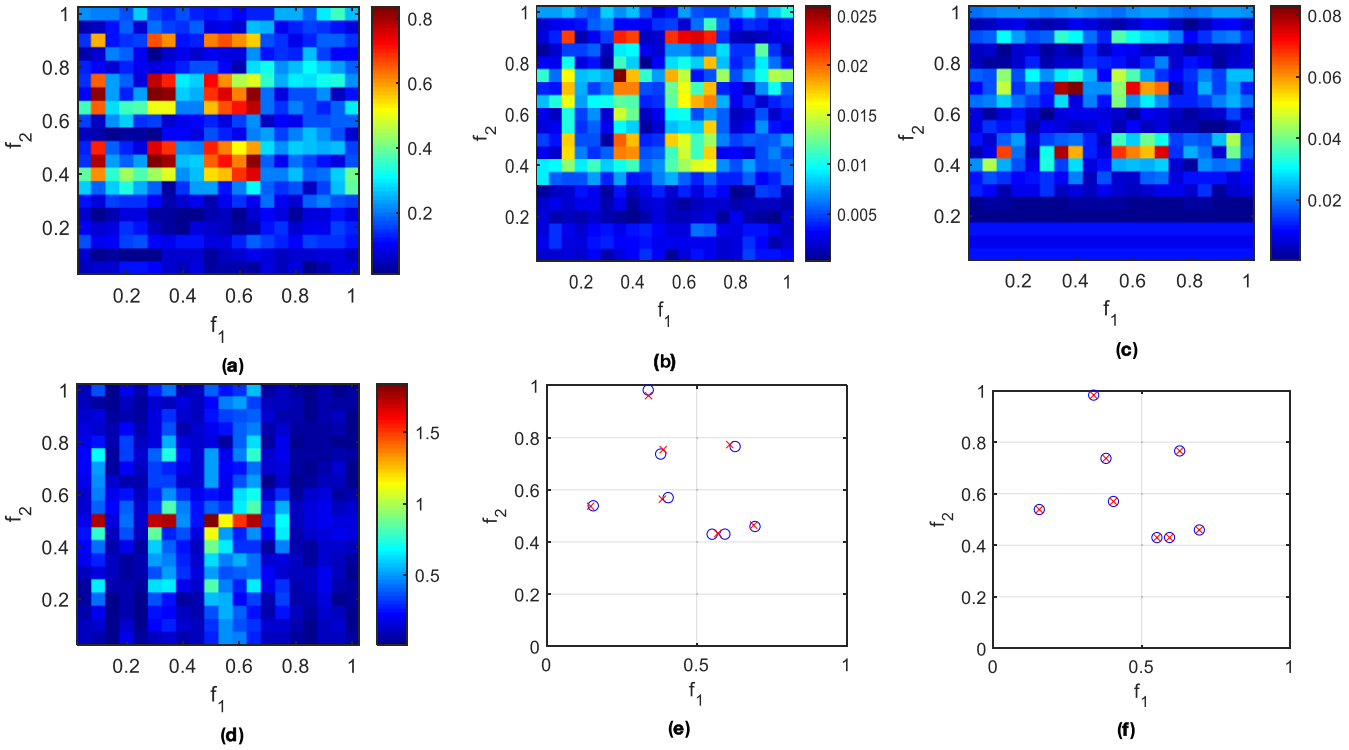

FIGURE 11. Spectrum estimation results of different methods. (a) Direct 2D-FFT on defect data. (b) APES. (c) BCS. (d) FFT of recovered signal by RAM with multi-column calculation. (e) 2-D ANM over amplitude threshold 0.05. (f) Proposed method over amplitude threshold 0.05.

thus lower SINR means more salient interference feature. The interference length is set as 40% of whole echo length. The result is shown in Figure 9 (b), where SINR of interference region has little effect on both ANM and RAM, because they have been processed by l_1 norm filtering from the beginning. Consistent with integrity rate, number of snapshots can affect RMSE similarly. More snapshot means more information to utilize, and better performance.

The experiment results show that for the situation that signal has not been entirely covered by TRFI, the RAM-based line spectrum estimation method will show its advantage in accuracy.

The results is consistent with [32] since we have transform the TRFI problem in dechirping radar into a typical sparse recovery problem. In this case, we apply the RAM for this typical line spectrum estimation problem over sparse signal and demonstrate its feasibility.

B. SIMULATION OF 2-D DATA

In this case, considering the exponentially increasing complexity $O((n_1 n_2)^{4.5})$ of 2-D ANM-based algorithm with computing points $n_1 n_2$, we cannot implement the algorithm in the actual sampled data block yet. However, we can still conduct a simulation referring [34] to test the proposed weighting strategy for 2-D signal block.

We simulate a small sample block of 2-D signal data with 8 associated frequencies after filtering, which shows a sparse form. Locations of (f_1, f_2) is shown in Figure 10 (a). The two points in red rectangular box are very close to each other, which will be a trouble for frequency recovery. The real position of (f_1, f_2) is $[(f_1, f_2)]$ =[(0.551,0.429), (0.404,0.570), (0.694,0.459), (0.628,0.766), (0.379,0.737), (0.155,0.538), (0.338,0.982),(0.594, 0.430)] and amplitude of each point is set as 1.

The size of collected filtered signal block is 20×20 with 30% of each column assumed to be interfered by TRFI with random position, which has been set as 0. The amplitude of collected defect signal block is shown in Figure 10 (b).

Figure 11 shows some 2-D frequency estimation results based on several typical algorithms, where (a) is direct 2D-FFT on defect data; (b) is Bayesian compressive sensing (BCS) [37] algorithm; (c) is amplitude and phase estimation (APES) [38] method; (d) is the 2D-FFT result of recovered signal by RAM, which is calculated through line spectrum estimation of each row; (e) Method of [34], which is based on ANM without an iterative calculation of SDP solver;(f) Proposed method. There are some low amplitude points in original estimation results of (e) and (f), which have bad influence on conciseness of final figures and have been filtered by an amplitude threshold of 0.05.

The comparison between Figure 11 (e) and (f) shows effect of promoting. In Figure 11 (e), the estimation accuracy is limited by the inadequate signal length, which is not as high as the reweighting method in almost all frequency positions. For the two points that are close to each other in red rectangular box of Figure 10 (a), original 2-D ANM cannot distinguish them, whereas the proposed weighting method performs better.

As shown in Figure 11, the proposed 2D-RAM method performs best accuracy in this case, mostly because of the iteration algorithm and weighting strategy. What needs to point is that the promoted accuracy of proposed method is at the cost of computing complexity, which needs several iterative solutions of SDP.

V. CONCLUSION

We have observed the interference phenomenon of TRFI and detailly explained the interfering mechanism from the basic of dechirping. Based on that, we have presented in this paper a simple yet very effective filtering method based on l_1 norm of STFT, which transforms original problem into a typical sparse signal recovery problem. We further implement a weighting strategy to promote the ANM for 2D data. We confirm the validity of our framework via an experiment of real measured signal in TRFI environment and a simulation of 2D echo data.

In the future work, further algorithms to reduce calculation complexity should be considered.

APPENDIX

The conclusion of (23) is given by fallowing equations.

$$\begin{aligned}
&\min_{\boldsymbol{U}} \frac{\sqrt{n_1 n_2}}{2}\mathrm{tr}\left(\boldsymbol{W}T(\boldsymbol{U})\right) + \frac{1}{2\sqrt{n_1 n_2}}\mathrm{tr}\left(z^H T\left(\boldsymbol{U}\right)^{-1} z\right)\\
&\text{s.t. } T\left(\boldsymbol{U}\right) \geq \boldsymbol{0}\\
&\quad = \min_{f_{1q},f_{2q},p_q\geq 0} \frac{\sqrt{n_1 n_2}}{2}\mathrm{tr}\left(\boldsymbol{W}\boldsymbol{R}\right) + \frac{1}{2\sqrt{n_1 n_2}}\mathrm{tr}\left(z^H \boldsymbol{R}^{-1} z\right)\\
&\qquad \text{s.t. } \boldsymbol{R} = \sum_q p_q \boldsymbol{a}(f_{1q},f_{2q})\boldsymbol{a}(f_{1q},f_{2q})^H\\
&\quad = \min_{f_{1q},f_{2q},p_q\geq 0,\sigma_q} \frac{\sqrt{n_1 n_2}}{2}\sum_q p_q \boldsymbol{a}(f_{1q},f_{2q})^H \boldsymbol{W}\boldsymbol{a}(f_{1q},f_{2q})\\
&\qquad + \frac{1}{2\sqrt{n_1 n_2}}\left\|\sigma_q\right\|_2^2 p_q^{-1}\\
&\qquad \text{s.t. } z = \sum_q \boldsymbol{a}(f_{1q},f_{2q})^H \sigma_q\\
&\quad = \min_{f_{1q},f_{2q},\sigma_q} w\left(f_{1q},f_{2q}\right)^{-1}\left\|\sigma_q\right\|_2 \ \text{s.t.} z = \sum_q \boldsymbol{a}(f_{1q},f_{2q})^H \sigma_q\\
&\qquad = \|z\|_{\mathcal{A}^w}
\end{aligned}$$

where the Vandermonde decomposition of $T(\boldsymbol{U})$ is applied in first derivation.

REFERENCES

[1] B. H. Kirk, R. M. Narayanan, K. A. Gallagher, A. F. Martone, and K. D. Sherbondy, "Avoidance of time-varying radio frequency interference with software-defined cognitive radar," *IEEE Trans. Aerosp. Electron. Syst.*, vol. 55, no. 3, pp. 1090–1107, Jun. 2019.

[2] Y. Huang, L. Zhang, J. Li, W. Hong, and A. Nehorai, "A novel tensor technique for simultaneous narrowband and wideband interference suppression on single-channel SAR system," *IEEE Trans. Geosci. Remote Sens.*, vol. 57, no. 12, pp. 9575–9588, Dec. 2019.

[3] H. Liu, D. Li, Y. Zhou, and T.-K. Truong, "Joint wideband interference suppression and SAR signal recovery based on sparse representations," *IEEE Geosci. Remote Sens. Lett.*, vol. 14, no. 9, pp. 1542–1546, Sep. 2017.

[4] H. Liu, D. Li, Y. Zhou, and T.-K. Truong, "Simultaneous radio frequency and wideband interference suppression in SAR signals via sparsity exploitation in time–frequency domain," *IEEE Trans. Geosci. Remote Sens.*, vol. 56, no. 10, pp. 5780–5793, Oct. 2018.

[5] S. Zhang, M. Xing, R. Guo, L. Zhang, and Z. Bao, "Interference suppression algorithm for SAR based on time–frequency transform," *IEEE Trans. Geosci. Remote Sens.*, vol. 49, no. 10, pp. 3765–3779, Oct. 2011.

[6] F. Zhou, M. Tao, X. Bai, and J. Liu, "Narrow-band interference suppression for SAR based on independent component analysis," *IEEE Trans. Geosci. Remote Sens.*, vol. 51, no. 10, pp. 4952–4960, Oct. 2013.

[7] F. Zhou, M. Xing, X. Bai, G. Sun, and Z. Bao, "Narrow-band interference suppression for SAR based on complex empirical mode decomposition," *IEEE Geosci. Remote Sens. Lett.*, vol. 6, no. 3, pp. 423–427, Jul. 2009.

[8] F. Zhou, R. Wu, M. Xing, and Z. Bao, "Eigensubspace-based filtering with application in narrow-band interference suppression for SAR," *IEEE Geosci. Remote Sens. Lett.*, vol. 4, no. 1, pp. 75–79, Jan. 2007.

[9] Y. Huang, G. Liao, L. Zhang, Y. Xiang, J. Li, and A. Nehorai, "Efficient narrowband RFI mitigation algorithms for SAR systems with reweighted tensor structures," *IEEE Trans. Geosci. Remote Sens.*, vol. 57, no. 11, pp. 9396–9409, Nov. 2019.

[10] Y. Huang, L. Zhang, J. Li, Z. Chen, and X. Yang, "Reweighted tensor factorization method for SAR narrowband and wideband interference mitigation using smoothing multiview tensor model," *IEEE Trans. Geosci. Remote Sens.*, vol. 58, no. 5, pp. 3298–3313, May 2019.

[11] H. Liu and D. Li, "RFI suppression based on sparse frequency estimation for SAR imaging," *IEEE Geosci. Remote Sens. Lett.*, vol. 13, no. 1, pp. 63–67, Jan. 2016.

[12] Z. Liu, G. Liao, and Z. Yang, "Time variant RFI suppression for SAR using iterative adaptive approach," *IEEE Geosci. Remote Sens. Lett.*, vol. 10, no. 6, pp. 1424–1428, Nov. 2013.

[13] L. H. Nguyen, T. Tran, and T. Do, "Sparse models and sparse recovery for ultra-wideband SAR applications," *IEEE Trans. Aerosp. Electron. Syst.*, vol. 50, no. 2, pp. 940–958, Apr. 2014.

[14] L. H. Nguyen and T. D. Tran, "Efficient and robust RFI extraction via sparse recovery," *IEEE J. Sel. Topics Appl. Earth Observ. Remote Sens.*, vol. 9, no. 6, pp. 2104–2117, Jun. 2016.

[15] X. Y. Wang, W. D. Yu, X. Y. Qi, and Y. Liu, "RFI suppression in SAR based on approximated spectral decomposition algorithm," *Electron. Lett.*, vol. 48, no. 10, pp. 594–596, May 2012.

[16] F. Zhou and M. Tao, "Research on methods for narrow-band interference suppression in synthetic aperture radar data," *IEEE J. Sel. Topics Appl. Earth Observ. Remote Sens.*, vol. 8, no. 7, pp. 3476–3485, Jul. 2015.

[17] L. Stankovic, I. Orovic, S. Stankovic, and M. Amin, "Compressive sensing based separation of nonstationary and stationary signals overlapping in time-frequency," *IEEE Trans. Signal Process.*, vol. 61, no. 18, pp. 4562–4572, Sep. 2013.

[18] B. Zhao, L. Huang, J. Li, and P. Zhang, "Target reconstruction from deceptively jammed single-channel SAR," *IEEE Trans. Geosci. Remote Sens.*, vol. 56, no. 1, pp. 152–167, Jan. 2018.

[19] L. A. Fang, Z. X. Hua, L. J. Hui, and L. Zhong, "The ISAR range profile compensation of fast-moving target using the dechirp method," *J. Astronaut.*, vol. 2, no. 5, pp. 1619–1623, 2004.

[20] R. J. C. Middleton, "Dechirp-on-receive linearly frequency modulated radar as a matched-filter detector," *IEEE Trans. Aerosp. Electron. Syst.*, vol. 48, no. 3, pp. 2716–2718, Jul. 2012.

[21] R. Baraniuk and P. Steeghs, "Compressive radar imaging," in *Proc. IEEE Radar Conf.*, Apr. 2007, pp. 128–133.

[22] O. Batu and M. Cetin, "Parameter selection in sparsity-driven SAR imaging," *IEEE Trans. Aerosp. Electron. Syst.*, vol. 47, no. 4, pp. 3040–3050, Oct. 2011.

[23] E. Giusti, D. Cataldo, A. Bacci, S. Tomei, and M. Martorella, "ISAR image resolution enhancement: Compressive sensing versus state-of-the-art super-resolution techniques," *IEEE Trans. Aerosp. Electron. Syst.*, vol. 54, no. 4, pp. 1983–1997, Aug. 2018.

[24] X. He, N. Tong, and W. Feng, *High-Resolution ISAR Imaging of Maneuvering Targets Based on the Sparse Representation of Multiple Column-Sparse Vectors*. New York, NY, USA: Academic, 2016.

[25] X. He, X. Hu, and N. Tong, "Two-dimension gradient projection method for sparse matrix reconstruction," *Electron. Lett.*, vol. 52, no. 17, pp. 1493–1495, Aug. 2016.

[26] X. He, N. Tong, and X. Hu, "Dynamic ISAR imaging of maneuvering targets based on sparse matrix recovery," *Signal Process.*, vol. 134, pp. 123–129, May 2017.

[27] X. Hu, N. Tong, Y. Guo, and S. Ding, "MIMO radar 3-D imaging based on multi-dimensional sparse recovery and signal support prior information," *IEEE Sensors J.*, vol. 18, no. 8, pp. 3152–3162, Apr. 2018.
[28] X. Hu, N. Tong, Y. Zhang, X. He, and Y. Wang, "Moving target's HRRP synthesis with sparse frequency-stepped chirp signal via atomic norm minimization," *IEEE Signal Process. Lett.*, vol. 23, no. 9, pp. 1212–1215, Sep. 2016.
[29] Y. Chi and M. F. Da Costa, "Harnessing sparsity over the continuum: Atomic norm minimization for superresolution," *IEEE Signal Process. Mag.*, vol. 37, no. 2, pp. 39–57, Mar. 2020.
[30] X. He, N. Tong, X. Hu, and W. Feng, "Radar pulse completion and high-resolution imaging with SAs based on reweighted ANM," *IET Signal Process.*, vol. 12, no. 7, pp. 868–872, Sep. 2018.
[31] B. Li, W. Bai, G. Zheng, and X. He, "RAM-based angle estimation with linear spatially separated polarisation sensitive array," *Int. J. Electron.*, vol. 105, no. 10, pp. 1657–1672, Oct. 2018.
[32] Z. Yang and L. Xie, "Enhancing sparsity and resolution via reweighted atomic norm minimization," *IEEE Trans. Signal Process.*, vol. 64, no. 4, pp. 995–1006, Feb. 2016.
[33] Z. Yang and L. Xie, "Achieving high resolution for super-resolution via reweighted atomic norm minimization," in *Proc. IEEE Int. Conf. Acoust., Speech Signal Process. (ICASSP)*, Apr. 2015, pp. 3646–3650.
[34] Y. Chi and Y. Chen, "Compressive two-dimensional harmonic retrieval via atomic norm minimization," *IEEE Trans. Signal Process.*, vol. 63, no. 4, pp. 1030–1042, Feb. 2015.
[35] G. Tang, B. N. Bhaskar, P. Shah, and B. Recht, "Compressed sensing off the grid," *IEEE Trans. Inf. Theory*, vol. 59, no. 11, pp. 7465–7490, Nov. 2013.
[36] Z. Yang and L. Xie, "Fast convex optimization method for frequency estimation with prior knowledge in all dimensions," *Signal Process.*, vol. 142, pp. 271–280, Jan. 2018.
[37] W. Wang and B. Zhang, "Adaptive sampling with Bayesian compressive sensing in radar sensor networks and image," *EURASIP J. Wireless Commun. Netw.*, vol. 2012, no. 1, p. 257, Dec. 2012.
[38] X. Bai, F. Zhou, M. Xing, and Z. Bao, "High-resolution radar imaging of air targets from sparse azimuth data," *IEEE Trans. Aerosp. Electron. Syst.*, vol. 48, no. 2, pp. 1643–1655, Apr. 2012.

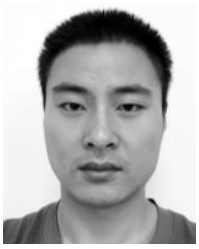

PENGCHENG WAN received the B.S. degree in radar engineering from Air Force Engineering University, Xi'an, China, in 2016, where he is currently pursuing the Ph.D. degree in electronic science and technology. His current research interests include radar imaging and radio frequency suppression.

NINGNING TONG received the B.S., M.S., and Ph.D. degrees from Air Force Engineering University, Xi'an, China, in 1984, 1988, and 2009, respectively. She is currently a Professor with Air Force Engineering University. She has authored or coauthored over 60 research articles and four books. Her current research interests include wireless communications, radar signal processing, and electronic countermeasures.

GUIMEI ZHENG (Member, IEEE) received the B.Eng. degree in biomedical engineering and the Ph.D. degree in signal and information processing from Xidian University, China, in 2009 and 2014, respectively. From 2015 to 2017, he was a full-time Postdoctoral Research Fellow with Tsinghua University, Beijing, China. He is currently a Lecturer with Air Force Engineering University, Xi'an, China. His research interests include MIMO radar and vector sensor array signal processing.